

Comprehensive Studies for Arbitrary-shape Scene Text Detection

Pengwen Dai^{1,2}, Xiaochun Cao^{1,2}

¹SKLOIS, Institute of Information Engineering, CAS, Beijing, China

²School of Cyber Security, University of Chinese Academy of Sciences, Beijing, China

{daipengwen, caoxiaochun}@iie.ac.cn

Abstract

Numerous scene text detection methods have been proposed in recent years. Most of them declare they have achieved state-of-the-art performances. However, the performance comparison is unfair, due to lots of inconsistent settings (e.g., training data, backbone network, multi-scale feature fusion, evaluation protocols, etc.). These various settings would dissemble the pros and cons of the proposed core techniques. In this paper, we carefully examine and analyze the inconsistent settings, and propose a unified framework for the bottom-up based scene text detection methods. Under the unified framework, we ensure the consistent settings for non-core modules, and mainly investigate the representations of describing arbitrary-shape scene texts, e.g., regressing points on text contours, clustering pixels with predicted auxiliary information, grouping connected components with learned linkages, etc. With the comprehensive investigations and elaborate analyses, it not only cleans up the obstacle of understanding the performance differences between existing methods, but also reveals the advantages and disadvantages of previous models under fair comparisons.

1. Introduction

Reading texts in the natural image is a hot topic, due to its wide practical applications, e.g., robot navigation [11], image caption [28], image retrieval [12], etc. Scene text detection, as the prerequisite of reading text system, has attracted increasing attention in the computer vision community over the past few years. However, due to the uneven illumination, the perspective distortion and the complex backgrounds in natural scenes, they result in the difficulties of detecting scene texts. Moreover, the specific characteristics of texts (e.g., various scales, diverse aspect ratios, different fonts, arbitrary-shape layouts, etc.) also increase the challenge of the detection.

To address these challenges, some existing methods [39, 15, 50, 10, 32, 14] adopt axis-aligned rectangles, ro-



Figure 1: Illustration of different representations for text instances. (a) Axis-aligned rectangle. (b) Rotated rectangle. (c) Quadrangle. (d) Arbitrary-shape contour.

tated rectangles or quadrangles to localize scene texts. Despite their progress on horizontal or multi-oriented texts, these methods may fall short, when handling arbitrary-shape texts that are ubiquitous in the real life, as shown in Figure 1 (a)(b)(c). To accurately localize arbitrary-shape text contours in the natural image (Figure 1 (d)), two kinds of methods are prevalent in the field of scene text detection. One is top-down based methods. They perform the binary segmentation or the regression of arbitrary-shape text contour points on the proposals. The other is bottom-up based methods. They first predict local units (e.g., pixels, connected components) and their auxiliary information, and then group them into different text instances.

However, it is hard to affirm whether and how a newly proposed model has the improvement in performance and speed, when comparing with previous same-type methods. It is because existing methods adopt different training settings and testing environments. As shown in Table 1 and Table 2, existing methods usually employ different backbone networks and utilize different external data to pre-train the model. We also observe that different testing scales would distinctly influence the performance and speed of the model. Moreover, some methods even claim they have achieved the state-of-the-arts based on the reported performance using different evaluation protocols (Table 2). These inconsisten-

cies hinder the fair comparisons between the proposed core techniques of existing methods.

In this paper, we make comprehensive studies for the bottom-up based methods, as this kind of methods has excellent speeds and owns more flexible representations for describing arbitrary-shape scene texts compared with top-down based methods. To reveal the advantages and disadvantages of the core techniques in existing methods, we propose a unified framework for the bottom-up based arbitrary-shape scene text detection, providing a common perspective for existing methods. Specifically, the proposed framework consists five consecutive operation modules. The first module is image pre-processing, which mainly refers to the data augmentation in the training stage and the image resizing in the testing stage. The second module is extracting visual features, using the backbone network pre-trained on ImageNet [27]. The third is the feature fusion module, which fuses multi-scale features to obtain better feature representations. The fourth module is the prediction head, which outputs estimated parameters of describing arbitrary-shape texts. The fifth module refers to the post-processing, which is only utilized in the testing stage. We thus could use this unified framework to support all existing bottom-up based scene text detectors. Based on the proposed framework, we investigate the influence of the fourth module (namely, the prediction head) under the unified experimental settings (*e.g.*, the same image pre-processing, backbone network and feature fusion strategy), as almost bottom-up based arbitrary-shape scene text detectors pay attention on this module. With this investigation, we can clearly understand the strengths and weaknesses of existing bottom-up based arbitrary-shape scene text detection methods. Meanwhile, it also exposes some overlooked explorations and challenges, which could guide more flourishing studies in the future works.

The contributions of this paper are summarized as follows: i) We reveal the inconsistencies between previous arbitrary-shape scene text detection methods, which help readers to perceive the advances and challenges in the field of the arbitrary-shape scene text detection. ii) A unified framework is introduced, which would facilitate comprehensive investigations for better understanding the pros and cons of existing detectors. iii) We provide a fair comparison toolkit, which would clean up the obstacle on the current comparisons.

2. Related Work

Arbitrary-shape scene text detection methods [21, 2] with deep learning can be roughly grouped into top-down methods and bottom-up methods.

Top-down arbitrary-shape scene text detectors: These detectors either carry out the binary segmentation or regress key contour points based on proposals. For

the segmentation-based methods, they usually perform the pixel-wise semantic segmentation for all pixels in the proposals, inspired by the framework of MaskRCNN [7], and mainly focus on enriching the feature representations or obtaining better segmentation [42, 19, 13, 46, 41, 4, 17]. For example, MS-CAFA [4] exploits a pyramid ROI pooling attention mechanism to learn robust features for proposals with various scales. Mask-TTD [17] adopts a tightness prior to adjust text proposals for better covering the entire text region, and utilizes the text frontier information to improve the text mask prediction. Moreover, in ContourNet [38], the authors only perform the segmentation for text contours on the adaptive proposals. For the regression-based methods [18, 3, 37], they directly or dynamically regress the key points on text contours. For example, CTD-CLOC [18] predicts the offsets of key points to the top-left points, and utilizes the Long Short-Term Memory (LSTM) to smooth the offsets. Instead of the static regression, ATRR [37] adaptively outputs the point pair using LSTM.

However, the top-down based methods usually require the artificial design of anchors, which would limit the generalization abilities of models for texts with various scales and aspect ratios. Besides, these methods involve multiple pipelines and complex networks, making them hard to achieve the promising speed.

Bottom-up Arbitrary-shape Scene Text Detectors: These detectors can be divided into pixel-wise based methods and component-wise based methods. The former ones [35, 30, 45, 36, 16, 34, 51, 31, 44, 47] predict the auxiliary information of each pixel or the specific pixel in the entire/shrunk text region to better formulate different text instances. For example, PSENet [35] introduces a progressive scale expansion algorithm to fuse multi-shrunk segmentation maps with the help of text region kernels. Similarly, PAN [36] estimates the embedding vectors of pixels to measure the distances to different text kernels. Besides, MSR [45] and TextField [44] learn the offset field of each pixel in text regions for better linking neighbor pixels. Furthermore, TextRay [31] predicts the text center heatmap and multiple rays rooted at the specific text center pixels, which can directly reconstruct the text instances and thus avoid the clustering process.

Differently, the component-wise based methods [22, 1, 29, 48, 23] first generate the local components based on the pixel-wise predictions, and then focus on exploring the grouping strategies (*e.g.*, heuristic rules, linkage estimation, relationship reasoning, etc.). For example, TextSnake [22] reconstructs entire text instances by sliding a circle along the central axis. Instead of the offline reconstruction, ICG [29] regards the linkages between the estimated rotated squares as a binary classification, to dynamically formulate the entire text instance. Moreover, DRRGN [48] and Re-LaText [23] further deduce the relationships between local

Type	Method	Venue	Backbone	Pretrain data	training data	testing size	IOU@0.5			FPS	GPUs (#)	
							R (%)	P (%)	F (%)			
Top-down based methods	CSE [19]	CVPR'19	ResNet34	MLT17+TD500+CTW+TOT	CTW	N/A	76.0	81.1	78.4	2.6	GTX 1080Ti (2)	
	ATTR [37]	CVPR'19	SE-VGG16	×	CTW	720×1280	80.2	80.1	80.1	10.0	Nvidia P40 (1)	
	CTC-CLOC [18]	PR'19	ResNet50	SynText	CTW	(600,1000)	69.8	77.4	73.4	13.3	GTX 1080 (1)	
	TextFuseNet [46]	IJCAI'20	ResNet50	SynText	CTW	1000 △	85.0	85.8	85.4	7.3	Tesla V100 (4)	
			ResNet101				85.4	87.8	86.6	3.7		
	ContourNet [38]	CVPR'20	ResNet50	×	CTW	720×1280	84.1	83.7	83.9	4.5	TiTan X (1)	
	SDM [40]	ECCV'20	ResNet50	MLT17→TOT	CTW	768 ◇	82.3	85.8	84.0	N/A	N/A	
							MS	84.4	88.4			86.4
	Poly-FRCNN-3 [3]	IJDAR'20	Inception-ResNet-v2	SynText→COCO-Text	CTW	N/A	(600, 800)	62.0	86.0	72.0	N/A	N/A
MS-CAFA [4]	TMM'20	ResNet50	×	CTW	MS	83.3	86.1	84.6	1.0	GTX 1080Ti (1)		
						85.1	85.7	85.4	N/A			
Mask-TTD [17]	TIP'20	ResNet50-FPN	×	CTW	N/A		79.0	79.7	79.4	N/A	Tesla P100 (1)	
Bottom-up based methods	TextSnake [22]	ECCV'18	VGG16	SynText	CTW	original size	85.3	67.9	75.6	N/A	TiTan X (2)	
	MSR [45]	IJCAI'19	ResNet50	SynText	CTW	MS	78.3	85.0	81.5	N/A	GTX 1080Ti (2)	
	SAE [30]	CVPR'19	ResNet50	SynText	CTW	800 ◇	77.8	82.7	80.1	N/A	TiTan X (1)	
	CRAFT [1]	CVPR'19	VGG16-BN	SynText	CTW	1024 ◇	81.1	86.0	83.5	N/A	N/A	
	LOMO [47]	CVPR'19	ResNet50	SynText	CTW	512 ◇	69.6	89.2	78.4	4.4	Tesla K40m (4)	
							MS	76.5	85.7	80.8		N/A
	PSENet-1s [35]	CVPR'19	ResNet50	×	CTW	1280 ◇	75.6	80.6	78.0	3.9	N/A (4)	
				MLT17			79.7	84.8	82.2	3.9		
	PSENet-4s [35]			MLT17			77.8	82.1	79.9	8.4		
	PAN [36]	ICCV'19	ResNet18	×	CTW	320 △	72.6	82.2	77.1	84.2	GTX 1080Ti (4)	
							512 △	77.1	83.8	80.3		58.1
					640 △		77.7	84.6	81.0	39.8		
				SynText	CTW		320 △	77.4	82.7	79.9		84.2
						512 △	81.5	85.5	83.5	58.1		
						640 △	81.2	86.4	83.7	39.8		
	TextDragon [5] ‡	ICCV'19	VGG16	SynText	CTW	N/A		82.8	84.5	83.6	N/A	GTX Titan X (1)
	SAST [34]	MM'19	ResNet50	SynText	CTW	512 ◇	77.1	85.3	81.0	27.6	TiTan Xp (4)	
							MS	81.7	81.2	81.5		N/A
	ICG [29]	PR'19	VGG16	SynText	CTW	512 △	79.8	82.8	81.3	N/A	Tesla P100 (1)	
AB-LSTM [20]	TOMM'19	VGG16	MLT17	CTW	N/A	81.6	83.0	82.3	N/A	GTX 1080Ti (1)		
TextField [44]	TIP'19	VGG16	SynText	CTW	576×576	79.8	83.0	81.4	N/A	TiTan Xp (1)		
DB [16]	AAAI'20	ResNet18-DCN	SynText	CTW	1024 *	77.5	84.8	81.0	55.0	GTX 1080Ti (1)		
		ResNet50-DCN				80.2	86.9	83.4	22.0			
TextPerceptron [25] ‡	AAAI'20	ResNet50	SynText	CTW	1250 ◇	81.9	87.5	84.6	N/A	Tesla V100 (8)		
DRRGN [48]	CVPR'20	VGG16	MLT17	CTW	(512,1024)	83.0	85.9	84.5	N/A	RTX 2080Ti (1)		
CRNet [51]	MM'20	ResNet50	SynText	CTW	1536 ◇	80.9	87.0	83.8	N/A	TiTan X (1)		
						MS	82.0	86.6			84.2	
TextRay [31]	MM'20	ResNet50	×	CTW	(640,800)	80.4	82.8	81.6	N/A	TiTan X (4)		
ReLaText [23]	PR'21	ResNet50	SynText	CTW	800 ◇	83.3	86.2	84.8	10.6	Nvidia V100 (4)		

Table 1: Comparisons between existing methods on the dataset CTW [18]. △, ◇ and * denote the short side, the long side and the height, respectively, when resizing the image with keeping the aspect ratio. (s_{min} , s_{max}) indicates the short side is set to s_{min} if it is less than s_{min} , and keep the longer side is not larger than s_{max} . ‡ means using the recognition branch to optimize the detection in an end-to-end framework. ‘MS’ represents the multi-scale testing. The red italic and the blue bold denote the optimal value for top-down based methods and bottom-up based methods respectively.

components with the graph convolution network.

These bottom-up based methods have more flexible representation of describing texts, and can usually achieve competitive performances and decent speed. Thus, they have become more and more prevalent. In this paper, we present a unified framework for the bottom-up arbitrary-scene text detectors, which is helpful to the fair comparison in the field of scene text detection.

3. Inconsistencies Analyses

In this section, we illustrate the different settings between prior works in details.

Backbones: As shown in Table 1 and Table 2, previous methods utilize different backbone networks (e.g.,

VGG16, ResNet50, ResNet101, etc.) pre-trained on ImageNet [27] to extract visual features. Stronger ones usually bring better performances. For example, in DB [16], using ResNet50 with deformable convolution networks (termed as ‘ResNet50-DCN’) as the backbone has the improvement of 2.4% in F -measure, compared with ResNet18-DCN. Similarly, using ResNet101 also increases the F -measure of 1.2% than using ResNet50 in TextFuseNet [46]. Even though some works adopt the same backbone networks, different versions of networks may also influence the performance. For example, PAN [36] uses the ResNet-v2 [9]¹ while other methods usually adopt ResNet-v1 [8].

Training Data: Some existing methods directly train

¹We found this from their official code: https://github.com/zhongqianli/pan_pp_pytorch

Type	Method	Venue	Backbone	Pretrain data	training data	testing size	DetEval-v1			FPS	GPUs (#)
							R (%)	P (%)	F (%)		
Top-down based methods	SPCNet [42]	AAAI'19	ResNet50	SynText→MLT17	TOT	N/A	82.8	83.0	82.9	N/A	N/A (8)
	CSE [19]	CVPR'19	ResNet34	MLT17+TD500+CTW+TOT	TOT	N/A	79.1	81.4	80.2	2.4	GTX 1080Ti (2)
	ATRR [37]	CVPR'19	SE-VGG16	×	TOT	(720,1280)	76.2	80.9	78.5	10.0	Nvidia P40 (1)
	MaskRCNN-OCR [26] ‡	ICCV'19	ResNet50	SynText+COCO-Text+IC15+MLT17+PD	TOT	600 △	83.4	83.3	83.3	N/A	Tesla V100 (15)
			Inception-ResNet	×	TOT	(600,1000)	85.0	87.8	86.4	N/A	
	CTC-CLOC [18]	PR'19	ResNet50	SynText	TOT	(600,1000)	71.0	74.0	73.0	N/A	GTX 1080 (1)
	Poly-FRCNN-3 [3]	IJDAR'20	Inception-ResNet-v2	SynText→COCO-Text	TOT	N/A	59.0	68.0	63.0	3.3	N/A
	Poly-FRCNN-3 [3] ♣	IJDAR'20	Inception-ResNet-v2	SynText→COCO-Text	TOT	N/A	68.0	78.0	73.0	3.3	N/A
	Poly-FRCNN-3 [3] ♠	IJDAR'20	Inception-ResNet-v2	SynText→COCO-Text	TOT	N/A	70.0	80.0	75.0	3.3	N/A
	Mask-TextSpotter [13] ♣	TPAMI'19	ResNet50-FPN	SynText	TOT	N/A	75.4	81.8	78.5	N/A	TiTan Xp (1)
	Mask-TextSpotter [13] ♠	TPAMI'19	ResNet50-FPN	SynText	TOT	N/A	82.4	88.3	85.2	N/A	TiTan Xp (1)
	Boundary [33] ‡	AAAI'20	ResNet50	SynText	TOT	1100 ◊	85.0	88.9	87.0	N/A	TiTan Xp (> 1)
	ContourNet [38]	CVPR'20	ResNet50	×	TOT	(720,1280)	83.9	86.9	85.4	3.8	TiTan X (1)
	TextFuseNet [46]	IJCAI'20	ResNet50	×	TOT	1000 △	83.2	87.5	85.3	7.1	Tesla V100 (4)
			ResNet101	SynText	TOT	1000 △	85.3	89.0	87.1	3.3	
SDM [40]	ECCV'20	ResNet50	MLT17	TOT	1024 ◊	84.7	89.2	86.9	N/A	N/A	
MS-CAFA [4]	TMM'20	ResNet50	×	TOT	(600,800)	74.7	83.5	78.9	0.8	GTX 1080Ti (1)	
			SynText	TOT	(600,800)	78.6	84.6	81.5			
Mask-TTD [17]	TIP'20	ResNet50-FPN	×	TOT	N/A	74.5	79.1	76.7	N/A	Tesla P100 (1)	
Bottom-up based methods	TextSnake [22]	ECCV'18	VGG16	SynText	TOT	512×512	74.5	82.7	78.4	N/A	TiTan X (2)
	CRAFT [1]	CVPR'19	VGG16-BN	SynText	TOT	1280 ◊	79.9	87.6	83.6	N/A	N/A
	LOMO [47]	CVPR'19	ResNet50	SynText	TOT	512 ◊	75.7	88.6	81.6	N/A	Tesla K40m (4)
						MS	79.3	87.6	83.3	N/A	
	PSENet-1s [35] ♠	CVPR'19	ResNet50	×	TOT	1280 ◊	75.1	81.8	78.3	3.9	N/A (4)
				MLT17	TOT	1280 ◊	78.0	84.0	80.9	3.9	
	PSENet-4s [35] ♠			MLT17	TOT	1280 ◊	75.2	84.5	79.6	8.4	
	MSR [45]	IJCAI'19	ResNet50	SynText	TOT	MS	74.8	83.8	79.0	N/A	GTX 1080Ti (2)
	PAN [36]	ICCV'19	ResNet18	×	TOT	320 △	71.3	84.0	77.1	82.4	GTX 1080Ti (4)
				×	TOT	512 △	78.4	86.7	82.4	57.1	
				×	TOT	640 △	79.4	88.0	83.5	39.6	
				SynText	TOT	320 △	75.0	85.6	79.9	82.4	
				×	TOT	512 △	79.7	89.4	84.3	57.1	
				×	TOT	640 △	81.0	89.3	85.0	39.6	
	TextDragon [5] ‡	ICCV'19	VGG16	SynText	TOT	N/A	75.7	85.6	80.3	N/A	GTX Titan X (1)
	CharNet [43] ‡	ICCV'19	Hourglass-57	SynText	TOT	N/A	81.0	88.6	84.6	N/A	N/A (8)
			Hourglass-88	SynText	TOT	N/A	81.7	89.9	85.6	N/A	
	SAST [34]	MM'19	ResNet50	SynText	TOT	512 ◊	76.9	83.8	80.2	N/A	TiTan Xp (4)
					MS	75.5	85.6	80.2	N/A		
ICG [29]	PR'19	VGG16	SynText	TOT	768 △	80.9	82.1	81.5	N/A	Tesla P100 (1)	
AB-LSTM [20] ♠	TOMM'19	VGG16	MLT17	TOT	N/A	78.2	78.9	78.5	N/A	GTX 1080Ti (1)	
TextField [44] ♠	TIP'19	VGG16	SynText	TOT	768×768	79.9	81.2	80.6	N/A	TiTan Xp (1)	
DB [16]	AAAI'20	ResNet18-DC	SynText	TOT	800 ×	77.9	88.3	82.8	50.0	GTX 1080 Ti (1)	
		ResNet50-DC	SynText	TOT	800 ×	82.5	87.1	84.7	32.0		
TextPerceptron[25] ‡	AAAI'20	ResNet50	SynText	TOT	1350 ◊	81.8	88.8	85.2	N/A	Tesla V100 (8)	
DRRGNet [48]	CVPR'20	VGG16	MLT17	TOT	(512,1280)	84.9	86.5	85.7	N/A	RTX 2080Ti (1)	
CRNet [51]	MM'20	ResNet50	SynText	TOT	1536 ◊	82.5	85.8	84.1	N/A	TiTan X (1)	
					MS	84.2	85.1	84.6			
TextRay[31] ♠	MM'20	ResNet50	×	TOT	960×960	77.9	83.5	80.6	N/A	TiTan X (4)	
ReLaText [23]	PR'21	ResNet50	SynText	TOT	1000 ◊	83.1	84.8	84.0	3.2	Nvidia V100 (4)	

Table 2: Comparisons between existing methods on the dataset TOT [3]. ♠ and ♣ denote evaluating the performance with the metric [3] IOU@0.5 and DetEval-v2 respectively.

the model on the real-world training data. Differently, some methods first utilize the synthetic dataset SynText [49] or the large-scale real-world dataset (*e.g.*, MLT17 [24], COCO-Text [6], etc.) to pre-train the model, and then the model is fine-tuned on the real-world training data. Table 1 and Table 2 have shown that pre-training on external data can bring obvious performance improvements. For example, pre-training on MLT17 achieves the improvement of 4.2% in *F-measure* for PSENet-1s [35] (Table 1). Similarly, pre-training SynText has elevated the *F-measure* of about 2.9% in PAN [36] (Table 1). Besides, different pre-training data and epochs may also result in different detection performances obviously, but existing methods usually does

not care about these inconsistencies, when comparing with other methods.

Testing Scales: In the inference stage, various testing sizes of the input image can obviously affect the performance and speed of the model, as displayed in Table 1 and Table 2. For example, in PAN [36] that does not pre-train on SynText, with the increase of the short size of the input image, the *F-measure* increases by 3.8% and 5.1% on the datasets CTW and TOT, respectively. Moreover, some methods even use the multi-scale testing strategy to promote the performance. However, they may only have a slight improvement on performance but consequently bring the decrease in speed. For example, the recent work CRNet [51]

with the multi-scale testing strategy (Table 1) only increases 0.3% in F -measure, compared with the previous method ContourNet [38] using the single-scale testing strategy.

Evaluation Protocols: When evaluating on TOT [3], it involves three kinds of evaluation protocols (*e.g.*, IOU@0.5, DetEval-v1 and DetEval-v2). However, some of existing methods do not indicate which kind of the evaluation protocol they use, which makes the comparison confusing. Moreover, prior works report the performances (Table 2) under different evaluation protocols, and make comparisons with each other. Thus, these comparisons are unreasonable, making the assertion of achieving state-of-the-arts unbelievable for some methods.

Data Augmentation: Scene text detection methods with deep neural networks are data-driven. Data augmentation thus plays significant roles in learning robust models. However, different data augmentation strategies may cause the performance change of the model in complex scenarios. For example, previous methods randomly crop the sub-image from the input image with different sizes (*e.g.*, 512×512 [34], 640×640 [30, 35, 16], 768×768 [44], 960×960 [31], etc.), which may make the model have different generalization abilities to the scales of texts. Meanwhile, some existing methods randomly rotate the input image with different angles (*e.g.*, $\{0^\circ, 90^\circ, 180^\circ, 270^\circ\}$ [34], $[-10^\circ, 10^\circ]$ [35, 16], etc.), pursuing the robustness to the rotated arbitrary-shape scene texts.

Multi-scale Feature Fusion: Deep arbitrary-shape scene text detectors usually involve fusing multi-scale features generated by the backbone network, before feeding into the prediction head. This fusion between low-level and high-level features could enrich the feature representations, facilitating the model to detect texts with various scales. However, existing methods usually introduce different fusion techniques, which further make trouble for fairly investigating the representations of describing texts. These different fusion techniques not only influence the performance, but also result in different memory and speed. Besides, even though the module adopts similar fusion strategies, it could still bring different performance gains, due to different resolutions of the output maps. For example, in PSENet [35], when the resolution of the output map is 1/4 of the input image (termed as ‘PSENet-4s’), it decreases by 2.3% and 1.3% in F -measure for the datasets CTW and TOT respectively, compared with ‘PSENet-1s’.

4. Proposed Unified Framework

In this section, we propose a unified framework for the bottom-up arbitrary-shape scene text detection methods, as shown in Figure 2. This framework mainly consists of five modules: image pre-processing, backbone, multi-scale feature fusion, prediction head and post-processing.

Specifically, the original image $\mathbf{I} \in \mathbb{R}^{H \times W \times 3}$ is first fed

into the image pre-processing module to generate the network input $\tilde{\mathbf{I}} \in \mathbb{R}^{\tilde{H} \times \tilde{W} \times 3}$, formulated as:

$$\tilde{\mathbf{I}} = \mathcal{N}(\mathcal{P}(\mathbf{I})), \quad (1)$$

where \mathcal{N} means the image normalization; \mathcal{P} refers to the data augmentation and the test image resizing strategy for the training and testing stage respectively. Due to the differences of \mathcal{P} in existing methods, we thus unify the settings of \mathcal{P} for fair comparisons following [48]. In the training stage, the data augmentation mainly involves four steps: i) Randomly scale the original image via the aspect ratio ranging in $[0.75, 2.5]$; ii) Randomly crop the image patch with the scale of 640×640 ; iii) Randomly rotate the cropped image patch with the angle of $[-90^\circ, 90^\circ]$. iv) Randomly flip the image in the horizontal direction with the probability of 0.5. In the testing stage, the test image resizing strategy indicates the short size of $\tilde{\mathbf{I}}$ is set to s if it is less than s , while the longer side is not larger than $2s$. In the experiments, s is set to 512 in default, and we also investigate the influence of performance against the change of s .

In the backbone module, we utilize the backbone network pre-trained on ImageNet [27] to extract multi-scale visual feature representations, which can be formulated as:

$$\{\mathbf{F}_i\}_{i=1}^L = \mathcal{B}(\tilde{\mathbf{I}}; \Theta_b), \quad (2)$$

where $\mathbf{F}_i \in \mathbb{R}^{(\tilde{H}/2^{i+1(i=1)}) \times (\tilde{W}/2^{i+1(i=1)}) \times D_i}$ denotes the feature map generated by the i -th stage of the backbone network \mathcal{B} with the pre-trained weights of Θ_b ; L is the number of multi-scale features; $\mathbb{1}$ means the indicator function. D_i is the dimension of the feature. In the framework, we adopt the frequently-used backbone network ResNet50 [8] like most existing scene text detection models.

Next, the feature fusion module ϕ combines low-level and high-level features for generating a more representative feature $\mathbf{F}^e \in \mathbb{R}^{(\tilde{H}/\sigma) \times (\tilde{W}/\sigma) \times D_e}$. It can be expressed as,

$$\mathbf{F}^e = \phi(\{\mathbf{F}_i\}_{i=1}^L; \Theta_f), \quad (3)$$

where σ and D_e denote the downsampling factor and dimension of feature maps; Θ_f indicates the learnable parameters in ϕ . Additionally, ϕ usually adopts a top-down fusion strategy. That is, it gradually fuses feature maps from deep semantic representations to shallow local cues. However, ϕ in most previous methods has obvious differences (More details can be seen in Section ?? of Appendix), which can result in different performances. To avoid the influence of different ϕ , we set the frequently-used fusion strategy like those in [22, 48], where σ is equal to 1.

After that, the enhanced feature \mathbf{F}^e is fed into a single prediction head module φ to estimate the local unit categories and their auxiliary information, termed as $\mathbf{Q} \in \mathbb{R}^{\frac{\sigma' \tilde{H}}{\sigma} \times \frac{\sigma' \tilde{W}}{\sigma} \times C_o}$, which can be formulated as :

$$\mathbf{Q} = \mathcal{U}_{\sigma'}(\varphi(\mathbf{F}^e; \Theta_p)), \quad (4)$$

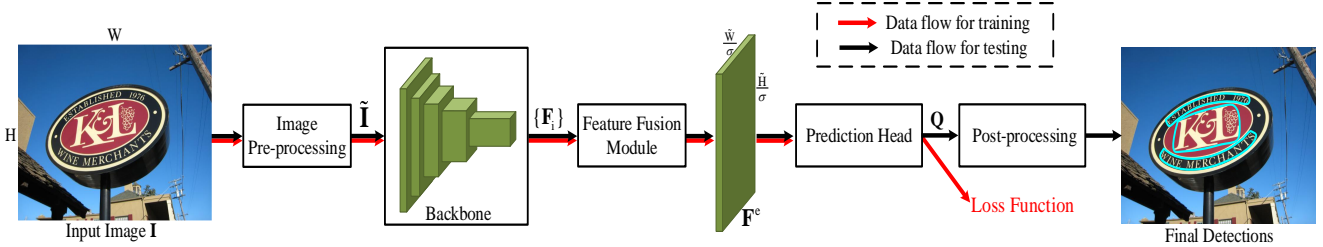


Figure 2: Illustration of the unified framework for the bottom-up arbitrary-shape scene detection models. Given an original input image \mathbf{I} , it is first pre-processed by the data augmentation in the training stage or the image resizing operation in the testing stage before the image normalization, generating the network input $\tilde{\mathbf{I}}$. Next, the backbone is utilized to extract multi-scale visual features $\{\mathbf{F}_i\}_{i=1}^L$, and then these multi-scale features are fused by the feature fusion module to obtain a more representative feature map \mathbf{F}^e . After that, \mathbf{F}^e is fed into the prediction head to generate the network outputs \mathbf{Q} . Finally, \mathbf{Q} is fed into the post-processing stage to obtain final detections in the testing stage, or is involved in the calculation of loss functions in the training stage.

Method	Venue	CTW							TOT						
		IOU@0.5			DetEval-v2			Speed (FPS)	IOU@0.5			DetEval-v2			Speed (FPS)
		R (%)	P (%)	F (%)	R (%)	P (%)	F (%)		R (%)	P (%)	F (%)	R (%)	P (%)	F (%)	
TextSnake [22]	ECCV'18	65.5	66.0	65.8	77.4	67.0	71.8	2.2	65.5	68.3	66.8	75.1	69.4	72.1	0.9
PSENet [35]	CVPR'19	74.9	84.6	79.5	71.1	78.8	75.3	15.1	70.3	81.1	75.3	70.8	77.2	73.9	10.3
PAN [36]	ICCV'19	58.7	89.6	70.9	74.8	89.9	81.7	9.5	73.0	88.8	80.1	75.7	89.0	81.8	9.3
DB [16]	AAAI'20	65.4	81.4	72.5	53.5	66.8	59.4	35.5	76.0	86.5	80.9	74.8	84.7	79.5	26.1
DRRGN [48]	CVPR'20	75.7	80.8	78.1	71.5	76.2	73.8	1.7	73.1	85.9	79.0	66.1	76.8	71.0	1.0

Table 3: Fair Comparisons of performances on two datasets CTW and TOT. The speed denotes the average over three runs.

where $\mathcal{U}_{\sigma'}$ indicates upsampling the resolution of the output with the factor of σ' . Θ_p denotes the learnable parameters in φ . C_o is the number of the prediction (e.g., categories and auxiliary information). For example, in PSENet [35], \mathbf{Q} consists of C_o segmentation masks for the text instances at different shrunk scales. It is worth noting that PSENet-1s ($\sigma'/\sigma = 4/4 = 1$) achieves better performance than PSENet-4s ($\sigma'/\sigma = 1/4$), due to different resolutions of the outputs. Similarly, \mathbf{Q} in DB [16] contains the predicted shrunk text region map and the estimated threshold map, and its resolution is also upsampled to the same as that of the network input ($\sigma'/\sigma = 4/4 = 1$) (More examples can be seen in Section ?? of Appendix). For a fair comparison, we set $\sigma' = \sigma$ in experiments.

After obtaining the network output \mathbf{Q} , it is directly fed into the loss function to calculate the loss in the training stage, or is post-processed to generate final detection results in the testing stage. Generally, most existing bottom-up arbitrary-shape scene text detectors mainly focus on the exploration of representations of describing text instances, which reflects at the prediction head module φ and its corresponding loss function.

5. Experiments and Analyses

With the unified framework, we emphatically investigate the prediction head module of several previous methods, for

profoundly disclosing the advances and shortages of current researches on arbitrary-shape scene text detection.

5.1. Datasets and Evaluation Protocols

CTW [18] is a prevalent arbitrary-shape scene text detection benchmark. It contains 1500 images (1000 images for training and 500 images for testing) in total. The annotation of the text instance is line-level, and is labeled by a polygon with 14 key points.

TOT [3] is also a frequently-used dataset for arbitrary-shape scene text detection. It consists of 1,255 training images and 300 testing images. The text instance in the image is annotated by the word-level polygon with unfixed number of key points.

For each dataset, we adopt two evaluation protocols, e.g., IOU@0.5 utilized in [18] and DetEval-v2 proposed in [3], for better revealing the performance differences.

5.2. Implementation details

Based on the official open codes, we adopt the same settings for the image pre-processing, backbone and feature fusion module to make a fair comparison. Other settings keep the same with the corresponding original methods. Additionally, the model is directly trained for 600 epochs on the training set of the corresponding dataset. The batch size is fixed to 6 in the training stage. When testing, the batch size is set to 1 in a single thread. All experiments



Figure 3: Qualitative detection results. The samples in the first row and the second row are from the dataset CTW and TOT respectively. The red bounding boxes denote detection results while the green bounding boxes are the ground-truth.

are conducted with the deep learning framework Pytorch 1.4, and on a workstation with a single RTX 2080Ti GPU, a 4.00GHz Intel(R) Xeon(R) W-2125 CPU, and 15G RAM.

5.3. Comparisons of Performance and Speed

Table 3 shows that PSENet [35] and PAN [36] achieve the optimal *F-measure* on CTW under the evaluation protocols IOU@0.5 and DetEval-v2 respectively. On the dataset TOT, DB [16] and PAN [36] have obtained the best *F-measure* under IOU@0.5 and DetEval-v2, respectively. In the terms of the speed, DB [16] significantly outperforms other methods. Meanwhile, the speed of the component-wise based methods TextSnake [22] and DRRGN [48] is distinctly slower than the pixel-wise based methods (e.g., PSENet [35], PAN [36], DB [16], etc.). Some visualized detection results are presented in Figure 3. These quantitative and qualitative experimental results indicate that an older method can be better than a newer method in performance or speed under fair comparisons. It is because the improvements in the original methods mainly come from some tricks (e.g., more training data, stronger backbone, well-designed feature fusion strategies, etc.). To further verify the ability of accurately localizing the text contours, we use stricter thresholds under the evaluation protocol IOU. As show in Figure 4, we observe that PAN [36] is more robust to the change of IOU threshold than other methods. Similarly, the qualitative results in Figure 3 have also shown that PAN [36] can achieve more accurate text contours.

5.4. Influence of Testing Scale

To investigate the robustness of scales, we validate several kinds of testing scales like those in [36]. As shown in Figure 5, it shows that different testing scales can result in obviously different performances. Even through the short

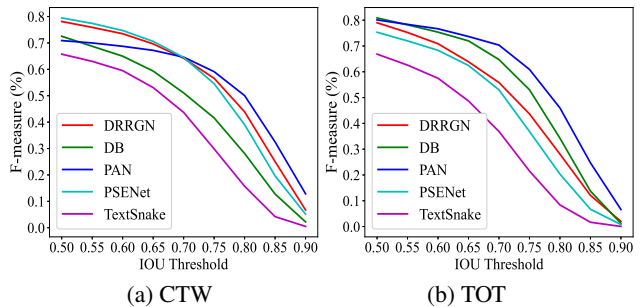


Figure 4: Performance changes against the IOU threshold in the evaluation protocol. The experiments are conducted on the datasets CTW (a) and TOT (b) for the detectors DRRGN [48], PAN [36], PSENet [35] and TextSnake [22]. Best view in color.

size s of the test image is consistent with the size (640×640) of the training image, it also can not ensure achieving the optimal performance. Under many conditions, it achieves the best performance, when using a smaller size (e.g., 512). The reason may be ascribed to the domain shift of the scale between the training data and the testing data. In effect, existing methods usually utilize the testing scale with no evidence. Sometimes, when we only change the testing scale, it would also bring an obvious performance improvement. In the past few years, learning a scale-robust detector for the arbitrary-shape scene texts with diversified scales and aspect ratios nearly draws little attention in the field of scene text detection.

5.5. Exploration of Generalization Ability

To verify the generalization ability of existing methods, we conduct cross-dataset experiments. Specifically, we train the models on the training set of CTW and then test on the testing set of TOT (CTW \rightarrow TOT), and vice versa (TOT

Method	Venue	CTW \rightarrow TOT						TOT \rightarrow CTW					
		IOU@0.5			DetEval-v2			IOU@0.5			DetEval-v2		
		R (%)	P (%)	F (%)	R (%)	P (%)	F (%)	R (%)	P (%)	F (%)	R (%)	P (%)	F (%)
TextSnake [22]	ECCV'18	29.6	36.6	32.7	65.3	47.9	55.3	57.3	44.8	50.3	73.5	71.8	72.6
PSENet [35]	CVPR'19	30.9	55.8	39.8	61.9	67.1	64.4	51.5	37.0	43.1	59.6	59.6	59.6
PAN [36]	ICCV'19	27.8	59.1	37.8	65.7	78.9	71.7	45.6	37.1	40.9	65.3	72.3	68.6
DB [16]	AAAI'20	29.2	60.0	39.3	45.1	65.0	53.3	53.4	35.4	42.6	65.6	71.3	68.3
DRRGN [48]	CVPR'20	32.4	55.3	40.9	64.6	66.1	65.3	50.9	36.0	42.2	56.8	57.9	57.3

Table 4: Generalization Ability.

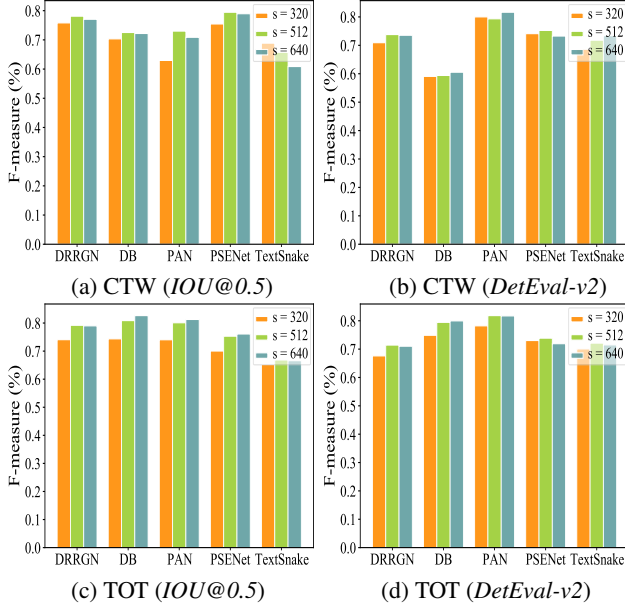


Figure 5: Effect of testing scales. The experiments are conducted on the datasets CTW and TOT for DRRGN [48], DB [16], PAN [36], PSENet [35] and TextSnake [22].

\rightarrow CTW). As shown in Table 4, we find that DRRGN [48] and PAN [36] can achieve the best F -measure on CTW \rightarrow TOT, under IOU@0.5 and DetEval-v2 respectively. Meanwhile, the older detector TextSnake [22] shows better generalization abilities on TOT \rightarrow CTW than other methods. These experiments further reveal that some older methods may still surpass the newly proposed methods in some aspects under fair comparisons.

5.6. Analyses of Convergence

As shown in Figure 6, it indicates that TextSnake [22] and PAN [36] can achieve more stable convergence, when evaluating under both IOU@0.5 and DetEval-v2. Meanwhile, TextSnake [22] also shows faster convergence than other methods. Figure 6 also shows that the convergence of the model is dependent on the evaluation protocol. For example, DRRGN [48] can achieve more stable convergence after about 200 epochs under IOU@0.5 than

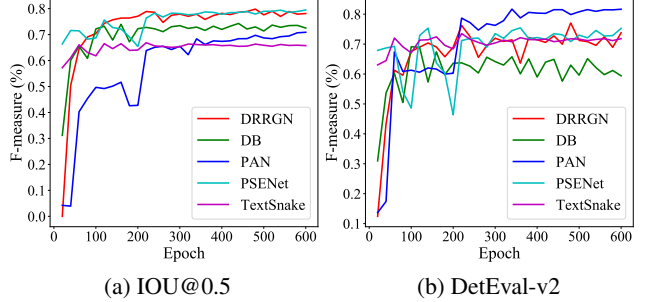


Figure 6: Illustration of the model convergence. The experiments are conducted on the dataset CTW for DRRGN [48], DB [16], PAN [36], PSENet [35] and TextSnake [22]. Best view in color.

DetEval-v2. Generally speaking, the stability and speed of the model convergence also reflect the advantages of the model to some extent, which is usually ignored by existing scene text detectors.

6. Conclusions

In this paper, we reveal the inconsistencies between existing arbitrary-shape scene text detectors. These inconsistencies bring difficulties in determining the advantages of the newly proposed core techniques compared with previous methods. To clean up the hindrance on fair comparisons, we present a unified framework for bottom-up arbitrary-shape scene text detection models. With this framework, we have provided a fair comparison for several well-known methods. We also provide comprehensive analyses on these methods for better disclosing their strengths and weaknesses. Thus, these profound studies suggest multiple directions to explore in the future. Firstly, it is necessary to propose more robust representations of describing arbitrary-shape scene texts with various scales and aspect ratios for more accurate localizations. Secondly, it is very meaningful to explore more efficient online data augmentation strategies by considering the intrinsic characteristics of scene texts. Thirdly, it is useful to study the scene text detector with a tradeoff between performance and speed on resource-constrained circumstances.

References

- [1] Youngmin Baek, Bado Lee, Dongyoon Han, Sangdoon Yun, and Hwalsuk Lee. Character region awareness for text detection. In *CVPR*, pages 9365–9374, 2019. 2, 3, 4
- [2] Xiaoxue Chen, Lianwen Jin, Yuanzhi Zhu, Canjie Luo, and Tianwei Wang. Text recognition in the wild: A survey. *ACM Computing Surveys*, In press, 2021. 2
- [3] Chee-Kheng Ch'ng, Chee Seng Chan, and Cheng-Lin Liu. Total-Text: toward orientation robustness in scene text detection. *Int. J. Document Anal. Recognit.*, 23(1):31–52, 2020. 2, 3, 4, 5, 6
- [4] Pengwen Dai, Hua Zhang, and Xiaochun Cao. Deep multi-scale context aware feature aggregation for curved scene text detection. *IEEE Trans. Multimedia*, 22(8):1969–1984, 2020. 2, 3, 4
- [5] Wei Feng, Wenhao He, Fei Yin, Xu-Yao Zhang, and Cheng-Lin Liu. TextDragon: An end-to-end framework for arbitrary shaped text spotting. In *ICCV*, pages 9075–9084, 2019. 3, 4
- [6] Raul Gomez, Baoguang Shi, Lluís Gomez-Bigorda, Lukas Neumann, Andreas Veit, Jiri Matas, Serge J. Belongie, and Dimosthenis Karatzas. ICDAR2017 robust reading challenge on COCO-Text. In *ICDAR*, pages 1435–1443, 2017. 4
- [7] Kaiming He, Georgia Gkioxari, Piotr Dollár, and Ross Girshick. Mask R-CNN. In *ICCV*, pages 2980–2988, 2017. 2
- [8] Kaiming He, Xiangyu Zhang, Shaoqing Ren, and Jian Sun. Deep residual learning for image recognition. In *CVPR*, pages 770–778, 2016. 3, 5
- [9] Kaiming He, Xiangyu Zhang, Shaoqing Ren, and Jian Sun. Identity mappings in deep residual networks. In *ECCV*, pages 630–645, 2016. 3
- [10] Wenhao He, Xu-Yao Zhang, Fei Yin, and Cheng-Lin Liu. Deep direct regression for multi-oriented scene text detection. In *ICCV*, pages 745–753, 2017. 1
- [11] Ziyang Hong, Yvan Petillot, David Lane, Yishu Miao, and Sen Wang. TextPlace: Visual place recognition and topological localization through reading scene texts. In *ICCV*, pages 2861–2870, 2019. 1
- [12] Sezer Karaoglu, Ran Tao, Theo Gevers, and Arnold W. M. Smeulders. Words Matter: Scene text for image classification and retrieval. *IEEE Trans. Multimedia*, 19(5):1063–1076, 2017. 1
- [13] Minghui Liao, Pengyuan Lyu, Minghang He, Cong Yao, Wenhao Wu, and Xiang Bai. Mask TextSpotter: An end-to-end trainable neural network for spotting text with arbitrary shapes. *IEEE Trans. Pattern Anal. Mach. Intell.*, In Press, 2019. 2, 4
- [14] Minghui Liao, Baoguang Shi, and Xiang Bai. TextBoxes++: A single-shot oriented scene text detector. *IEEE Trans. Image Process.*, 27(8):3676–3690, 2018. 1
- [15] Minghui Liao, Baoguang Shi, Xiang Bai, Xinggang Wang, and Wenyu Liu. TextBoxes: A fast text detector with a single deep neural network. In *AAAI*, pages 4161–4167, 2017. 1
- [16] Minghui Liao, Zhaoyi Wan, Cong Yao, Kai Chen, and Xiang Bai. Real-time scene text detection with differentiable binarization. In *AAAI*, pages 11474–11481, 2020. 2, 3, 4, 5, 6, 7, 8
- [17] Yuliang Liu, Lianwen Jin, and ChuanMing Fang. Arbitrarily shaped scene text detection with a mask tightness text detector. *IEEE Trans. Image Process.*, 29:2918–2930, 2020. 2, 3, 4
- [18] Yuliang Liu, Lianwen Jin, Shuaitao Zhang, and Sheng Zhang. Curved scene text detection via transverse and longitudinal sequence connection. *Pattern Recognit.*, 90:337–345, 2019. 2, 3, 4, 6
- [19] Zichuan Liu, Guosheng Lin, Sheng Yang, Fayao Liu, Weisi Lin, and Wang Ling Goh. Towards robust curve text detection with conditional spatial expansion. In *CVPR*, pages 7269–7278, 2019. 2, 3, 4
- [20] Zhandong Liu, Wengang Zhou, and Houqiang Li. AB-LSTM: Attention-based bidirectional lstm model for scene text detection. *ACM Transactions on Multimedia Computing, Communications, and Applications*, 15(4):1–23, 2019. 3, 4
- [21] Shangbang Long, Xin He, and Cong Yao. Scene text detection and recognition: The deep learning era. *Int. J. Comput. Vis.*, 129(1):161–184, 2021. 2
- [22] Shangbang Long, Jiaqiang Ruan, Wenjie Zhang, Xin He, Wenhao Wu, and Cong Yao. TextSnake: A flexible representation for detecting text of arbitrary shapes. In *ECCV*, pages 19–35, 2018. 2, 3, 4, 5, 6, 7, 8
- [23] Chixiang Ma, Lei Sun, Zhuoyao Zhong, and Qiang Huo. Re-LaTeX: Exploiting visual relationships for arbitrary-shaped scene text detection with graph convolutional networks. *Pattern Recognit.*, 111:107684, 2021. 2, 3, 4
- [24] Nibal Nayef, Fei Yin, Imen Bizid, and et al. ICDAR2017 robust reading challenge on multi-lingual scene text detection and script identification - RRC-MLT. In *ICDAR*, pages 1454–1459, 2017. 4
- [25] Liang Qiao, Sanli Tang, Zhanzhan Cheng, Yunlu Xu, Yi Niu, Shiliang Pu, and Fei Wu. Text Perceptron: Towards end-to-end arbitrary-shaped text spotting. In *AAAI*, pages 11899–11907, 2020. 3, 4
- [26] Siyang Qin, Alessandro Bissacco, Michalis Raptis, Yasuhisa Fujii, and Ying Xiao. Towards unconstrained end-to-end text spotting. In *ICCV*, pages 4703–4713, 2019. 4
- [27] Olga Russakovsky, Jia Deng, Hao Su, Jonathan Krause, Sanjeev Satheesh, Sean Ma, Zhiheng Huang, Andrej Karpathy, Aditya Khosla, Michael S. Bernstein, Alexander C. Berg, and Fei-Fei Li. Imagenet large scale visual recognition challenge. *Int. J. Comput. Vis.*, 115(3):211–252, 2015. 2, 3, 5
- [28] Oleksii Sidorov, Ronghang Hu, Marcus Rohrbach, and Amanpreet Singh. TextCaps: A dataset for image captioning with reading comprehension. In *ECCV*, pages 742–758, 2020. 1
- [29] Jun Tang, Zhibo Yang, Yongpan Wang, Qi Zheng, Yongchao Xu, and Xiang Bai. SegLink++: Detecting dense and arbitrary-shaped scene text by instance-aware component grouping. *Pattern Recognit.*, 96, 2019. 2, 3, 4
- [30] Zhuotao Tian, Michelle Shu, Pengyuan Lyu, Ruiyu Li, Chao Zhou, Xiaoyong Shen, and Jiaya Jia. Learning shape-aware embedding for scene text detection. In *CVPR*, pages 4234–4243, 2019. 2, 3, 5

- [31] Fangfang Wang, Yifeng Chen, Fei Wu, and Xi Li. TextRay: Contour-based geometric modeling for arbitrary-shaped scene text detection. In *ACM-MM*, pages 111–119, 2020. [2](#), [3](#), [4](#), [5](#)
- [32] Fangfang Wang, Liming Zhao, Xi Li, Xinchao Wang, and Dacheng Tao. Geometry-aware scene text detection with instance transformation network. In *CVPR*, pages 1381–1389, 2018. [1](#)
- [33] Hao Wang, Pu Lu, Hui Zhang, Mingkun Yang, Xiang Bai, Yongchao Xu, Mengchao He, Yongpan Wang, and Wenyu Liu. All You Need Is Boundary: Toward arbitrary-shaped text spotting. In *AAAI*, pages 12160–12167, 2020. [4](#)
- [34] Pengfei Wang, Chengquan Zhang, Fei Qi, Zuming Huang, Mengyi En, Junyu Han, Jingtuo Liu, Errui Ding, and Guangming Shi. A single-shot arbitrarily-shaped text detector based on context attended multi-task learning. In *ACM-MM*, pages 1277–1285, 2019. [2](#), [3](#), [4](#), [5](#)
- [35] Wenhai Wang, Enze Xie, Xiang Li, Wenbo Hou, Tong Lu, Gang Yu, and Shuai Shao. Shape robust text detection with progressive scale expansion network. In *CVPR*, pages 9336–9345, 2019. [2](#), [3](#), [4](#), [5](#), [6](#), [7](#), [8](#)
- [36] Wenhai Wang, Enze Xie, Xiaoge Song, Yuhang Zang, Wenjia Wang, Tong Lu, Gang Yu, and Chunhua Shen. Efficient and accurate arbitrary-shaped text detection with pixel aggregation network. In *ICCV*, pages 8439–8448, 2019. [2](#), [3](#), [4](#), [6](#), [7](#), [8](#)
- [37] Xiaobing Wang, Yingying Jiang, Zhenbo Luo, Cheng-Lin Liu, Hyunsoo Choi, and Sungjin Kim. Arbitrary shape scene text detection with adaptive text region representation. In *CVPR*, pages 6449–6458, 2019. [2](#), [3](#), [4](#)
- [38] Yuxin Wang, Hongtao Xie, Zhengjun Zha, Mengting Xing, Zilong Fu, and Yongdong Zhang. ContourNet: Taking a further step toward accurate arbitrary-shaped scene text detection. In *CVPR*, pages 11750–11759, 2020. [2](#), [3](#), [4](#), [5](#)
- [39] Dao Wu, Rui Wang, Pengwen Dai, Yueying Zhang, and Xiaochun Cao. Deep strip-based network with cascade learning for scene text localization. In *ICDAR*, pages 826–831, 2017. [1](#)
- [40] Shanyu Xiao, Liangrui Peng, Ruijie Yan, Keyu An, Gang Yao, and Jaesik Min. Sequential deformation for accurate scene text detection. In *ECCV*, pages 108–124, 2020. [3](#), [4](#)
- [41] Shanyu Xiao, Liangrui Peng, Ruijie Yan, Keyu An, Gang Yao, and Jaesik Min. Sequential deformation for accurate scene text detection. In *ECCV*, pages 108–124, 2020. [2](#)
- [42] Enze Xie, Yuhang Zang, Shuai Shao, Gang Yu, Cong Yao, and Guangyao Li. Scene text detection with supervised pyramid context network. In *AAAI*, pages 9038–9045, 2019. [2](#), [4](#)
- [43] Linjie Xing, Zhi Tian, Weilin Huang, and Matthew R. Scott. Convolutional character networks. In *ICCV*, pages 9125–9135, 2019. [4](#)
- [44] Yongchao Xu, Yukang Wang, Wei Zhou, Yongpan Wang, Zhibo Yang, and Xiang Bai. TextField: Learning A deep direction field for irregular scene text detection. *IEEE Trans. Image Process.*, 28(11):5566–5579, 2019. [2](#), [3](#), [4](#), [5](#)
- [45] Chuhui Xue, Shijian Lu, and Wei Zhang. MSR: multi-scale shape regression for scene text detection. In *IJCAI*, pages 989–995, 2019. [2](#), [3](#), [4](#)
- [46] Jian Ye, Zhe Chen, Juhua Liu, and Bo Du. TextFuseNet: Scene text detection with richer fused features. In *IJCAI*, pages 516–522, 2020. [2](#), [3](#), [4](#)
- [47] Chengquan Zhang, Borong Liang, Zuming Huang, Mengyi En, Junyu Han, Errui Ding, and Xinghao Ding. Look More Than Once: An accurate detector for text of arbitrary shapes. In *CVPR*, pages 10552–10561, 2019. [2](#), [3](#), [4](#)
- [48] Shi-Xue Zhang, Xiaobin Zhu, Jie-Bo Hou, Chang Liu, Chun Yang, Hongfa Wang, and Xu-Cheng Yin. Deep relational reasoning graph network for arbitrary shape text detection. In *CVPR*, pages 9696–9705, 2020. [2](#), [3](#), [4](#), [5](#), [6](#), [7](#), [8](#)
- [49] Zheng Zhang, Chengquan Zhang, Wei Shen, Cong Yao, Wenyu Liu, and Xiang Bai. Multi-oriented text detection with fully convolutional networks. In *CVPR*, pages 4159–4167, 2016. [4](#)
- [50] Xinyu Zhou, Cong Yao, He Wen, Yuzhi Wang, Shuchang Zhou, Weiran He, and Jiajun Liang. EAST: An efficient and accurate scene text detector. In *CVPR*, pages 2642–2651, 2017. [1](#)
- [51] Yu Zhou, Hongtao Xie, Shancheng Fang, Yan Li, and Yongdong Zhang. CRNet: A center-aware representation for detecting text of arbitrary shapes. In *ACM-MM*, pages 2571–2580, 2020. [2](#), [3](#), [4](#)